Research Article

Jing Gao#, Dongdong Jiao#, Linbo Zhang, Guanjun Xu*, Xue Deng, Qi Zang, Honglei Yang, Ruifang Dong*, Tao Liu*, and Shougang Zhang

Vibration sensitivity minimization of an ultra-stable optical reference cavity based on orthogonal experimental design

https://doi.org/10.1515/phys-2022-0269
received March 07, 2023; accepted June 19, 2023

Abstract: The ultra-stable optical reference cavity (USORC) is a key element for a variety of applications. In this work, based on the orthogonal experimental design method, we study the vibration sensitivity optimization of a classical USORC with a 100 mm length. According to a test of 4 levels and 3 factors, the L_{16} (4^3) orthogonal table is established to design orthogonal experiments. The vibration sensitivities under different parameters are simulated and analyzed. The vibration sensitivities in three directions of the USORC are used as three single-object values, and the normalized sum of the three vibration sensitivities is selected as comprehensive object values. Through the range analysis of the object values, the influence degrees of the parameters on the three single objects and the comprehensive object are determined. The optimal parameter combination schemes are obtained by using the comprehensive balance method and the comprehensive evaluation method, respectively. Based on the corresponding fractional frequency stability of ultra-stable lasers, the final optimal parameter combination scheme A1B3C3 is determined and verified. This work is the first to use an orthogonal experimental design method to optimize vibration sensitivities, providing an approach to vibration sensitivities optimization and is also beneficial for the vibration sensitivity design of a transportable USORC.

Keywords: ultra-stable optical reference cavity, optimization, vibration sensitivity, orthogonal experimental design, ultra-stable laser

1 Introduction

Ultra-stable lasers have important applications, such as high-precision spectroscopy, gravitational redshift measurement,

# These authors contributed equally to this work and should be considered first co-authors.

*** Corresponding author: Guanjun Xu,** National Time Service Center, Chinese Academy of Sciences, 3 East Shuyuan Road, Xi'an 710600, China; Key Laboratory of Time and Frequency Standards, Chinese Academy of Sciences, 3 East Shuyuan Road, Xi'an, China, 710600, e-mail: xuguanjun@ntsc.ac.cn
*** Corresponding author: Ruifang Dong,** National Time Service Center, Chinese Academy of Sciences, 3 East Shuyuan Road, Xi'an 710600, China; Key Laboratory of Time and Frequency Standards, Chinese Academy of Sciences, 3 East Shuyuan Road, Xi'an, China, 710600, e-mail: dongruifang@ntsc.ac.cn
*** Corresponding author: Tao Liu,** National Time Service Center, Chinese Academy of Sciences, 3 East Shuyuan Road, Xi'an 710600, China; Key Laboratory of Time and Frequency Standards, Chinese Academy of Sciences, 3 East Shuyuan Road, Xi'an, China, 710600, e-mail: taoliu@ntsc.ac.cn
Jing Gao: National Time Service Center, Chinese Academy of Sciences, 3 East Shuyuan Road, Xi'an 710600, China; Key Laboratory of Time and Frequency Standards, Chinese Academy of Sciences, 3 East Shuyuan Road, Xi'an, China, 710600, e-mail: gaojing@ntsc.ac.cn
Dongdong Jiao: National Time Service Center, Chinese Academy of Sciences, 3 East Shuyuan Road, Xi'an 710600, China; Key Laboratory of Time and Frequency Standards, Chinese Academy of Sciences, 3 East Shuyuan Road, Xi'an, China, 710600, e-mail: jiaodd@ntsc.ac.cn
Linbo Zhang: National Time Service Center, Chinese Academy of Sciences, 3 East Shuyuan Road, Xi'an 710600, China; Key Laboratory of Time and Frequency Standards, Chinese Academy of Sciences, 3 East Shuyuan Road, Xi'an, China, 710600, e-mail: linbo@ntsc.ac.cn
Xue Deng: National Time Service Center, Chinese Academy of Sciences, 3 East Shuyuan Road, Xi'an 710600, China; Key Laboratory of Time and Frequency Standards, Chinese Academy of Sciences, 3 East Shuyuan Road, Xi'an, China, 710600, e-mail: dengxue@ntsc.ac.cn
Qi Zang: National Time Service Center, Chinese Academy of Sciences, 3 East Shuyuan Road, Xi'an 710600, China; Key Laboratory of Time and Frequency Standards, Chinese Academy of Sciences, 3 East Shuyuan Road, Xi'an, China, 710600, e-mail: zangqi@ntsc.ac.cn
Honglei Yang: Science and Technology on Metrology and Calibration Laboratory, Beijing Institute of Radio Metrology and Measurement, 50 Yongding Road, Beijing 100854, China, e-mail: yhlpc@163.com
Shougang Zhang: National Time Service Center, Chinese Academy of Sciences, 3 East Shuyuan Road, Xi'an 710600, China; Key Laboratory of Time and Frequency Standards, Chinese Academy of Sciences, 3 East Shuyuan Road, Xi'an, China, 710600, e-mail: szhang@ntsc.ac.cn

relativistic test, gravitational wave detection, and coherent communication [1–6]. Currently, ultra-stable lasers are often achieved by using the Pound–Drever–Hall method based on an ultra-stable optical reference cavity (USORC) [7–15]. A USORC is the reference of the laser frequency, so the stability of the optical length of USORCs primarily determines the fractional frequency stability of ultra-stable lasers [7–10].

The main factors affecting the stability of the optical length of USORCs include vibration [9–24], temperature [25,26], and thermal noise [27–30], where the latter two can be well solved by controlling temperature and increasing USORC's length. In general, the index to assess the impact of vibration on the stability of the optical length of USORCs is vibration sensitivity [7–10]. In order to reduce this impact, the finite element method plays an important role [7–9]. Benefiting from this, the vibration sensitivity of USORC is reduced from 10^{-9}/g to 10^{-11}/g by the passive method [7–11,13–15,17–19]. Furthermore, the fractional frequency stability of state-of-the-art laboratory ultra-stable lasers [25,26] and transportable ultra-stable laser systems [14,19,22,23] approach an order of magnitude of 10^{-17} in 1 s and an order of magnitude of 10^{-16} in 1 s, respectively.

However, in order to design the USORC with low vibration sensitivity, a large number of numerical simulations are often required to obtain a better combination of parameters, and it is difficult to compare the influence degree of parameters on vibration sensitivity under the same conditions. In addition, with the improvement of ultra-stable laser performance requirements, it has changed from focusing mainly on vibration sensitivity in the vertical direction in the past to paying attention to the three directions (*X*-axis, *Y*-axis, and *Z*-axis). In this case, it is obviously very difficult to obtain the optimal parameter combination of the lowest vibration sensitivity in the three directions only by the commonly used single-factor and single-object analysis and calculation, as well as the commonly used observation method. The orthogonal experimental design method [31] can greatly reduce the number of tests without reducing the test feasibility. Through range analysis, the influence degree of each factor on the object can be obtained, and the optimal parameter combination required for the multi-object can be determined. The orthogonal experimental design method can be used to optimize the USORC's parameters to achieve the least vibration sensitivity, but as far as we know, related research has not been reported.

In this work, based on the orthogonal experimental design method with multi-object, we optimize the parameters of a classic cylindrical USORC with a 100 mm length to achieve the minimum effect induced by the vibration sensitivity. According to the vibration characteristics of the USORC, the finite element model of quasi-static mechanics is established to simulate and calculate the vibration sensitivities. The L_{16} (4^3) orthogonal table is adopted to design the orthogonal experiment based on a test of 4 levels and 3 factors including the position Zc of the support point in the *Z*-axis direction, the support point position Yp in the *Y*-axis direction, and the support pad area Ps. We simulate and analyze the vibration sensitivities under the three parameters. The vibration sensitivities in three directions are determined as three single-object values, and the normalized sum of the three vibration sensitivities is the comprehensive object value. Based on the range analysis, we analyze and discuss the influence degree of the three parameters on the object values. The optimal parameter combination schemes are obtained by using the comprehensive balance method and the comprehensive evaluation method, respectively. According to the corresponding fractional frequency stability of the ultra-stable laser, the final optimal parameter combination scheme A1B3C3 (Zc = 3 mm, Yp = 10 mm, and Ps = 3 mm) is determined and verified by the finite element method. This work provides a method of vibration sensitivities optimization for USORCs and is also beneficial for the vibration sensitivity design of a transportable USORC, which is affected by more factors.

This article is structured as follows: We present the design of the cylindrical USORC with a 100 mm length in Section 2. In Section 3, we design an orthogonal experiment including the determination of test indexes, design variables, orthogonal experimental table, and test results. Optimization of vibration sensitivity based on a comprehensive balance method and a comprehensive evaluation method is provided in Section 4. The final optimization results are determined in Section 4.3. The conclusions are summarized in Section 5.

2 Design of the USORC

In this work, we consider the cylindrical USORC designed by Millo *et al.* [7], which is widely used in related fields. The geometric model of the USORC is shown in Figure 1, which is supported by four square pads with a thickness of 1 mm. Both the length and diameter of the USORC are 100 mm. The diameter of the optical channel along the *Y*-axis is 10 mm. There are two mirrors with a diameter of 25.4 mm and a thickness of 6.3 mm. The venting hole with a 6 mm diameter is drilled in the upper half along the *Z*-axis. The position of the four support pads requires extensive calculation simulations to design the USORC with the lowest vibration sensitivity. Two square "cutouts" are machined along the *Y*-axis of the cylindrical spacer to provide the contact

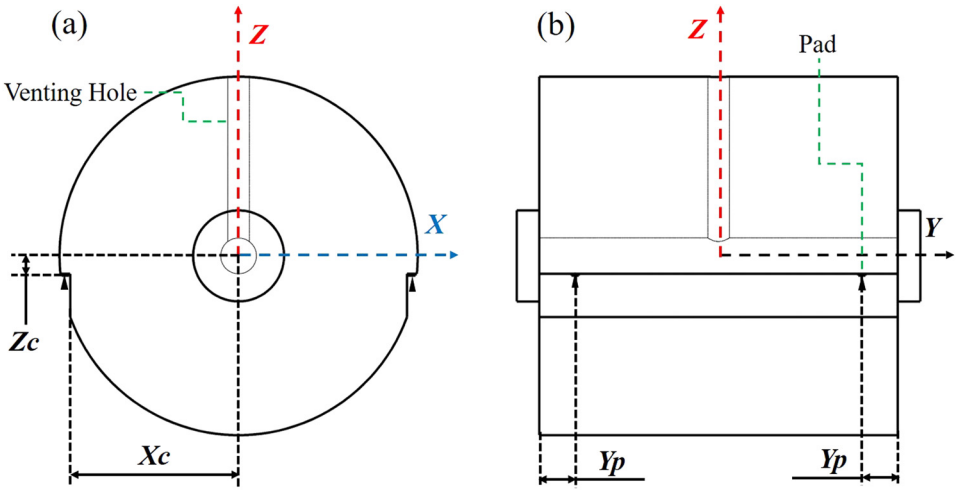

Figure 1: Geometric model of the cylindrical USORC [7]. Black triangles are used to indicate each of the four support points. (a) Front view and (b) side view.

planes for these support points. The four support pads are symmetrically distributed across the spacer and are all located on the same horizontal plane. To have the least vibration sensitivity, the USORC should ideally be a perfect cylinder supported at the horizontal midplane *XY*, with contact points placed on the surface of the USORC. Because the cavity and support points are entirely symmetrical, vibration will not result in mirror translations. Mirror translation owing to vertical vibration is no longer guaranteed by the symmetry as a result of the cutouts disrupting the cavity symmetry about the *XY* plane. For some cutout designs, the simulation can, however, be used to determine a specific location for the support points to achieve the least vibration sensitivity. The cuts for the support points are positioned as follows [7]: Xc with respect to the *YZ* plane and Zc with respect to the *XY* plane. The distance from the USORC's end along the *Y*-axis is indicated by Yp.

3 Test design

3.1 Simulation analysis model

The cylindrical USORC is analyzed by a quasi-static mechanical model, which is commonly used in the vibration sensitivity analysis [7–10,17–19]. The USORC is regarded as a single elastic body in the finite element analysis model. In the elastic limit, simulation deformations are determined. Elastic deformations of the USORC cause a cavity length change when the cavity is loaded by vibration acceleration. As shown in Table 1, the mechanical characteristics of the ultra-low expansion (ULE) glass have been used in simulation models. In order to save computational time, a quarter model is used in the calculation of vibration sensitivity along the *Z*-axis direction, and two half models are used in the analysis of vibration sensitivities along the *X*-axis and the *Y*-axis direction vibration. The geometry of the USORC is meshed with tetrahedral elements, where each tetrahedral element has 4 nodes and the side length of each tetrahedral element is about 1.5 mm. When calculating the vibration sensitivity, the USORC is subjected to 1 g of vibration acceleration. The calculation method of vibration sensitivity is based on the definition of Chen *et al.* [8].

3.2 Determination of test indexes

Vibration sensitivity (including *X*-axis, *Y*-axis, and *Z*-axis) is the key index of USORC. For the same material and the same shape of the USORC, different parameters have different influence rules on vibration sensitivities. The vibration sensitivities will eventually affect the stability of the ultra-stable laser. In this work, vibration sensitivities along three directions (S_z, S_x, and S_y) and the normalized sum (S) of the three vibration sensitivities are selected as three single-object values and comprehensive object values, respectively.

Table 1: Material properties of the USORC [7]

Material properties	Elastic modulus (GPa)	Poisson ratio	Density (kg/m^3)
ULE	67.6	0.17	2,210

3.3 Design variables and values

For the USORC in this work, the main parameters affecting the vibration sensitivities include the position of the support point in the *Z*-axis direction (Zc), the position of the support point in the *X*-axis direction (Xc), the position of the support point in the *Y*-axis direction (Yp), and the support pad area (Ps), which affect the USORC vibration sensitivities to varying degrees. In the optimization process of these parameters, the range of design variables is very important, which not only affects whether the selected range has an optimal solution or a suboptimal solution but also affects the search efficiency of the optimization process. Referring to the study by Millo *et al.* [7], the position of the support point in the *X*-axis direction (Xc) is 47 mm. In order to meet the requirements of minimum vibration sensitivities and better parameters, the range of design variables in Table 2 is adopted. There are three design variables, the position of the support point in the *Z*-axis direction (Zc), the position of the support point in the *Y*-axis direction (Yp), and the support pad area (Ps), each of which is divided into four levels. *A*, *B*, and *C* denote Zc, Yp, and Ps, respectively.

Table 2: Factors and levels of orthogonal test

Level	Position of support point in the *Z*-axis direction *A* Zc (mm)	Position of support point in the *Y*-axis direction *B* Yp (mm)	Support pad area *C* Ps (mm^2)
1	3	2	1
2	5	6	2
3	7	10	3
4	9	14	4

3.4 Orthogonal experimental table and test results

The test of all different combinations of test conditions is called a comprehensive test. In this test, the full-scale test contains 64 different combinations of tests, to be conducted one by one, which is obviously time-consuming and unnecessary. This work is a test of 3 factors and 4 levels. We select L_{16} (4^3) orthogonal table to design an orthogonal experiment, and only 16 tests are needed, which is 75% less than the comprehensive test. In the test, the vibration sensitivity values under the combination of different parameters are obtained. The test scheme and test results are shown in Table 3. S_z, S_x, and S_y present the absolute values of vibration sensitivities along three directions, *Z*-axis, *X*-axis, and *Y*-axis. The normalized sum of vibration sensitivities in three directions is represented by *S*, which is also the comprehensive object value. Generally, the vibration in the *Z*-axis direction is dominant in the laboratory environment [32–35]. Therefore, in the normalization process, it is assumed that S_z accounts for 80% and the other two items each account for 10%.

Table 3: Orthogonal table of experiment L_{16} (4^3) and simulation test data

Number	*A* Zc (mm)	*B* Yp (mm)	*C* Ps (mm^2)	S_z 10^{-10}/g	S_x 10^{-12}/g	S_y 10^{-12}/g	*S*
1	3	2	1	5.04	7.10	2.18	55.16
2	3	6	2	1.72	3.91	6.04	18.14
3	3	10	3	0.12	9.29	10.37	1.70
4	3	14	4	1.81	2.82	0.71	18.65
5	5	2	2	6.23	31.01	4.14	72.78
6	5	6	1	1.38	4.51	0.70	14.22
7	5	10	4	0.93	6.23	26.32	10.92
8	5	14	3	2.89	4.05	21.57	31.90
9	7	2	3	7.37	27.02	6.15	84.73
10	7	6	4	1.61	2.80	162.56	25.01
11	7	10	1	1.38	14.65	40.16	18.17
12	7	14	2	4.29	57.32	4.66	56.22
13	9	2	4	6.62	41.56	49.22	81.40
14	9	6	3	1.57	16.12	189.49	28.44
15	9	10	2	2.36	17.41	3.75	27.56
16	9	14	1	5.18	32.52	9.57	61.76

Table 4: Results of the ranges analysis of S_z

Mean values and ranges of level scores	Factors		
	A	*B*	*C*
$L_{1\text{-}1}$	8.69	25.26	12.98
$L_{2\text{-}1}$	11.43	6.28	14.6
$L_{3\text{-}1}$	14.65	4.79	11.95
$L_{4\text{-}1}$	15.73	14.17	10.97
$L_{1\text{-}1\text{-}M}$	2.17	6.32	3.25
$L_{2\text{-}1\text{-}M}$	2.86	1.57	3.65
$L_{3\text{-}1\text{-}M}$	3.66	1.20	2.99
$L_{4\text{-}1\text{-}M}$	3.93	3.54	2.74
D_1	1.76	5.12	0.91

4 Optimization of vibration sensitivity

To obtain the optimal parameter combination of minimum vibration sensitivities, a comprehensive balance method and a comprehensive evaluation method are adopted for the optimization of vibration sensitivity in this work. The optimization process is as follows: First, the optimal combinations of three single objects are obtained by range analysis, and then the global optimal combination is selected by the comprehensive balance method. Second, through the range analysis of the normalization *S*, the optimal combination of parameters is determined. According to the comparison of the corresponding fractional frequency stability of the ultra-stable laser based on the optimal parameter combination schemes (including the comprehensive balance method and comprehensive evaluation method), the final optimal parameter combination scheme is obtained.

4.1 Comprehensive balance method

The three vibration sensitivities (S_z, S_x, and S_y) are calculated and analyzed by single index one by one. For each vibration sensitivity index, the optimal combination of three design parameters is given. According to the importance of each vibration sensitivity index and the primary and secondary factors in each index, the overall optimal combination is finally determined. In this work, we use the range method to analyze the data to obtain the relationship between various factors and indicators.

Through the calculation and analysis of the range of the vibration sensitivity, the influence of various parameters on the vibration sensitivity S_z of the USORC is

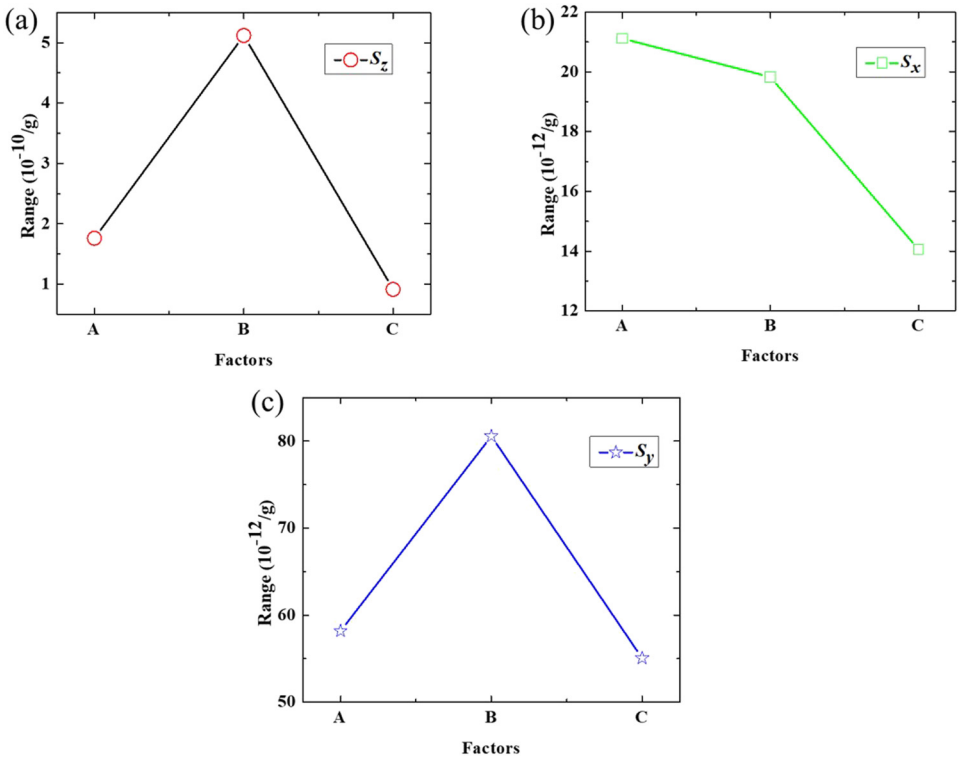

Figure 2: Range of the vibration sensitivity. (a) The *Z*-axis direction. (b) The *X*-axis direction. (c) The *Y*-axis direction.

obtained. The position Yp of the support point in the *Y*-axis direction has the greatest influence on vibration sensitivity S_z, and the support pad area Ps has the least influence on vibration sensitivity S_z, namely, $B > A > C$. The results are shown in Table 4 and Figure 2(a). In Table 4, $L_{1\text{-}1}$, $L_{2\text{-}1}$, $L_{3\text{-}1}$, and $L_{4\text{-}1}$ denote the sums of the vibration sensitivity S_z for four levels, respectively. $L_{1\text{-}1\text{-}M}$, $L_{2\text{-}1\text{-}M}$, $L_{3\text{-}1\text{-}M}$, and $L_{4\text{-}1\text{-}M}$ represent the means of $L_{1\text{-}1}$, $L_{2\text{-}1}$, $L_{3\text{-}1}$, and $L_{4\text{-}1}$, respectively. The range of the vibration sensitivity S_z is denoted by D_1. According to the requirements of the USORC, the smaller the vibration sensitivity S_z the better. The optimized combination of various parameters is *A*1*B*3*C*4, that is, the position Zc of the support point in the *Z*-axis direction is 3 mm, the position Yp of the support point in the *Y*-axis direction is 10 mm, the support pad area Ps is 4 mm^2.

As shown in Table 5 and Figure 2(b), the impact of different parameters on the vibration sensitivity S_x of the USORC is determined through the computation and examination of the vibration sensitivity range. In Table 5, the sums of the vibration sensitivity S_x for four levels are expressed as $L_{1\text{-}2}$, $L_{2\text{-}2}$, $L_{3\text{-}2}$, and $L_{4\text{-}2}$, respectively. The mean values of $L_{1\text{-}2}$, $L_{2\text{-}2}$, $L_{3\text{-}2}$, and $L_{4\text{-}2}$ are represented by $L_{1\text{-}2\text{-}M}$, $L_{2\text{-}2\text{-}M}$, $L_{3\text{-}2\text{-}M}$, and $L_{4\text{-}2\text{-}M}$, correspondingly. D_2 represents the range of the vibration sensitivity S_x. The support point's position Zc in the *Z*-axis direction has the biggest impact on vibration sensitivity S_x, while the support pad area Ps has the least vibration sensitivity S_x, with $A > B > C$ as the order of importance. The USORC requires that the vibration sensitivity S_x should be as low as possible. The optimal combination of different parameters is A1B2C4, which means that the support point's position Zc in the *Z*-axis direction is 3 mm, its position in the *Y*-axis direction is 6 mm, and the support pad area Ps is 4 mm^2.

As seen in Table 6 and Figure 2(c), the computation and analysis of the vibration sensitivity range are used to determine the effects of various factors on the USORC's vibration sensitivity S_y. The sums of the vibration sensitivity S_y are represented as $L_{1\text{-}3}$, $L_{2\text{-}3}$, $L_{3\text{-}3}$, and $L_{4\text{-}3}$ in Table 5, correspondingly, for four levels. $L_{1\text{-}3\text{-}M}$, $L_{2\text{-}3\text{-}M}$, $L_{3\text{-}3\text{-}M}$, and $L_{4\text{-}3\text{-}M}$, respectively, indicate the means of $L_{1\text{-}3}$, $L_{2\text{-}3}$, $L_{3\text{-}3}$, and $L_{4\text{-}3}$. The range of the vibration sensitivity S_y is represented by D_3. The most influence on vibration sensitivity S_y comes from the support point's position Yp along the *Y*-axis, while the least influence comes from the support pad area Ps, with $B > A > C$ being the order of significance. The vibration sensitivity S_y should meet the USORC's requirements for minimum values. The ideal arrangement of the various parameters is *A*1*B*4*C*2, which specifies that the support point's position Zc in the *Z*-axis direction, its position Yp in the *Y*-axis direction, and the support pad area Ps are 3 mm, 14 mm, and 2 mm^2, respectively.

In the vibration sensitivity analysis, the primary and secondary relationships of the three factors on the three indicators are: the vibration sensitivity S_z along the *Z*-axis direction: $B > A > C$; the vibration sensitivity S_x along the *X*-axis direction: $A > B > C$; the vibration sensitivity S_y along the *Y*-axis direction: $B > A > C$. The three optimal schemes: The optimal scheme with the lowest vibration sensitivity S_z

Table 6: Results of the ranges analysis of S_y

Means and ranges of level scores	Factors		
	A	*B*	*C*
$L_{1\text{-}3}$	19.3	61.69	52.61
$L_{2\text{-}3}$	52.73	358.79	18.59
$L_{3\text{-}3}$	213.53	80.6	227.58
$L_{4\text{-}3}$	252.03	36.51	238.81
$L_{1\text{-}3\text{-}M}$	4.83	15.42	13.15
$L_{2\text{-}3\text{-}M}$	13.18	89.70	4.65
$L_{3\text{-}3\text{-}M}$	53.38	20.15	56.90
$L_{4\text{-}3\text{-}M}$	63.01	9.13	59.70
D_3	58.18	80.57	55.05

Table 5: Results of the ranges analysis of S_x

Mean values and ranges of level scores	Factors		
	A	*B*	*C*
$L_{1\text{-}2}$	23.12	106.69	58.78
$L_{2\text{-}2}$	45.8	27.34	109.65
$L_{3\text{-}2}$	101.79	47.58	56.48
$L_{4\text{-}2}$	107.61	96.71	53.41
$L_{1\text{-}2\text{-}M}$	5.78	26.67	14.70
$L_{2\text{-}2\text{-}M}$	11.45	6.84	27.41
$L_{3\text{-}2\text{-}M}$	25.45	11.90	14.12
$L_{4\text{-}2\text{-}M}$	26.90	24.18	13.35
D_2	21.12	19.83	14.06

Table 7: Results of the ranges analysis of the comprehensive evaluation

Mean values and ranges of level scores	Factors		
	A	*B*	*C*
L_1	93.65	294.07	149.31
L_2	129.82	85.81	174.7
L_3	184.13	58.35	146.77
L_4	199.16	168.53	135.98
$L_{1\text{-}M}$	23.41	73.52	37.33
$L_{2\text{-}M}$	32.46	21.45	43.68
$L_{3\text{-}M}$	46.03	14.59	36.69
$L_{4\text{-}M}$	49.79	42.13	34.00
D	26.38	58.93	9.68

Table 8: Fractional frequency stability of the ultra-stable laser based on the above optimal schemes

Number	*A* Zc (mm)	*B* Yp (mm)	*C* Ps (mm^2)	S_z 10^{-10}/g	S_x 10^{-12}/g	S_y 10^{-12}/g	Relative frequency stability
*A*1*B*3*C*1	3	10	1	0.16	9.45	50.31	3.02×10^{-17}
*A*1*B*3*C*3	3	10	3	0.12	9.29	10.37	1.39×10^{-17}
*A*1*B*3*C*4	3	10	4	0.30	4.45	1.71	3.01×10^{-17}

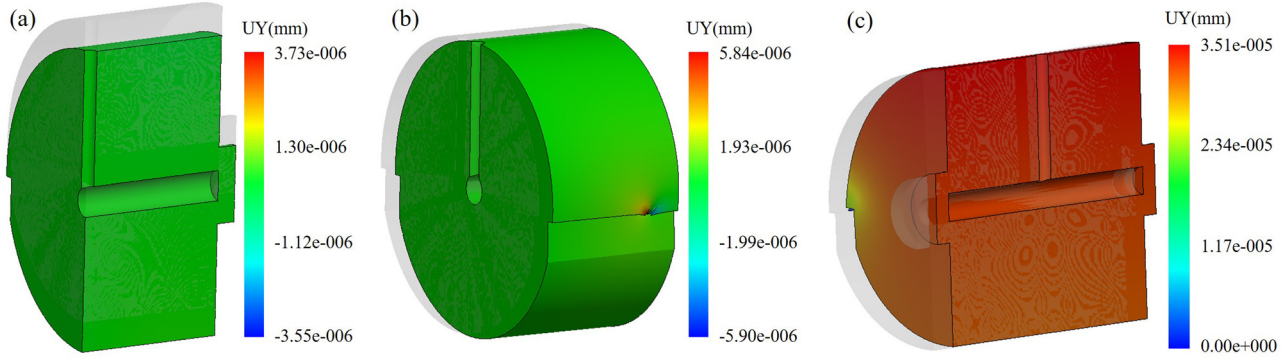

Figure 3: The USORC's displacement in the optical axis when the *A*1*B*3*C*3 is selected as the optimal combination. Note that the undeformed USORC is displayed in gray. (a) 1 g acceleration along the *Z*-axis direction. (b) 1 g acceleration along the *X*-axis direction. (c) 1 g acceleration along the *Y*-axis direction.

as the evaluation objective is *A*1*B*3*C*4; the optimal solution with the minimal vibration sensitivity S_x as the evaluation object is *A*1*B*2*C*4; and the optimal solution with the least vibration sensitivity S_y is *A*1*B*4*C*2. A1 is in all the three optimal schemes, so *A*1 is first determined. Factor *B* has a great influence on all three vibration sensitivities, and it has the greatest influence on the vibration sensitivities S_z and S_y, which should be analyzed first. Compared with the other two indicators, S_z is the most important indicator, so to ensure that it is the lowest first, *B*3 is selected. *C*4 appears in the optimal combination of the two optimal schemes, so *C*4 is selected. Finally, *A*1*B*3*C*4 is determined as the optimal combination by the comprehensive balance method.

4.2 Comprehensive evaluation method

Table 7 demonstrates how the computation and analysis of the comprehensive object values range are utilized to ascertain the influence of different parameters on the USORC's comprehensive object *S*. The *S* for the four levels are denoted in Table 7 as L_1, L_2, L_3, and L_4, respectively. The means of L_1, L_2, L_3, and L_4 are represented by $L_{1\text{-}M}$, $L_{2\text{-}M}$, $L_{3\text{-}M}$, and $L_{4\text{-}M}$, correspondingly. *D* represents the range of the comprehensive object *S*. The support point's position along the *Y*-axis, Yp, has the greatest impact on the overall object *S*, while the support pad area, Ps, has the least impact. $B > A > C$ is the order of significance. The minimum values of the USORC must be satisfied by the comprehensive object *S*. The effect of *C*1, *C*3, and *C*4 on comprehensive object *S* is basically the consistency. Eventually, *A*1*B*3*C*1, *A*1*B*3*C*3, and *A*1*B*3*C*4 are selected.

4.3 Optimization results

In order to obtain the final optimal scheme, we use the fractional frequency stability of the ultra-stable laser as the criterion indicator. The frequency relative variation in the laser due to the vibration sensitivity of a USORC can be expressed as follows [19,32]:

$$\frac{\Delta v}{v} = \left(\sum_{i=x,y,z} (S_i \times a_i)^2 \right)^{\frac{1}{2}}, \tag{1}$$

where v is the laser frequency, and Δv is the laser frequency change. We denote S_i as the sensitivities of the USORC length to vibration acceleration along the *X*-axis, *Y*-axis, or *Z*-axis.

Most laboratory environments have vibrations of approximately 1 μg (or even lower) [32–35], so it is assumed that the

vibration along the *Z*-axis direction is 1 μg and the vibration along the horizontal direction (*X*-axis and *Y*-axis) is 0.5 μg. According to Eq. (1), the fractional frequency stabilities of the ultra-stable laser based on the above optimal schemes are shown in Table 8.

According to Table 8, it is easy to understand that the *A*1*B*3*C*3 is the optimal scheme, and the corresponding fractional frequency stability of the ultra-stable laser is 1.39×10^{-17}. When the *A*1*B*3*C*3 is selected as the optimal combination, the USORC's displacement in the optical axis is shown in Figure 3.

5 Conclusion

The vibration sensitivity is one of the core performance indicators of USORCs. To get wonderful performances of ultra-stable lasers, the vibration sensitivity is required to be as low as possible. In this work, taking a classical USORC with a 100 mm length as an example, we optimize its vibration sensitivities by using the orthogonal experimental design method with multi-object. Based on a test of 3 factors (including the position Zc of the support point in the *Z*-axis direction, the position Yp of the support point in the *Y*-axis direction, and the support pad area Ps) and 4 levels, the L_{16} (4^3) orthogonal table is selected to design an orthogonal experiment. The vibration sensitivities under three important parameters are simulated and analyzed by the finite element method. We select the vibration sensitivity in three directions (*X*-axis, *Y*-axis, and *Z*-axis) as three single-object, and the comprehensive object value is the normalized sum of the three vibration sensitivities. According to the range analysis of the single-object value and the comprehensive object value, the influence degree of the three parameters on the object values is determined. The optimal parameter combination schemes are obtained by using the comprehensive balance method and the comprehensive evaluation method. By comparing the corresponding fractional frequency stability of the ultra-stable laser based on the above optimal parameter combination schemes, the final optimal parameter combination scheme is *A*1*B*3*C*3 (Zc = 3 mm, Yp = 10 mm, and Ps = 3 mm^2), which is also verified by the finite element method. As far as we know, this is the first time to use the orthogonal experimental design method with multi-object on vibration sensitivity optimization of UROSC and verify its effectiveness. This work aims to provide a reference for vibration sensitivities optimization of an USORC, especially a transportable USORC affected by more factors, such as a squeezing force, a length-to-diameter ratio, and weight.

Acknowledgments: The authors would like to acknowledge the contribution of X. Zhang of Northwestern Polytechnical University to this work.

Funding information: The project is partially supported by the Youth Innovation Promotion Association of the Chinese Academy of Sciences (Grant No. 1188000XGJ), the Chinese National Natural Science Foundation (Grant No. 11903041), and the Young Innovative Talents of the National Time Service Center of the Chinese Academy of Sciences (Grant No. Y917SC1).

Author contributions: Conceptualization: G.X. and J.G.; methodology: D.J.; software: J.G.; validation: D.J. and H.Y.; investigation: G.X.; data curation: J.G. and X.D.; writing – original draft preparation: G.X.; writing – review and editing: G.X. and J.G.; visualization: L.Z. and Q.Z.; supervision: R.D.; project administration: T.L. and S.Z. All authors have accepted responsibility for the entire content of this manuscript and approved its submission.

Conflict of interest: The authors state no conflict of interest.

References

[1] Predehl K, Grosche G, Raupach SMF, Droste S, Terra O, Alnis J, et al. A 920-kilometer optical fiber link for frequency metrology at the 19th decimal place. Science. 2012;336:441–4.
[2] Kennedy CJ, Oelker E, Robinson JM, Bothwell T, Kedar D, Milner WR, et al. Precision metrology meets cosmology: improved constraints on ultralight dark matter from atom-cavity frequency comparisons. Phys Rev Lett. 2020;125:201302.
[3] Müller H, Peters A, Chu S. A precision measurement of the gravitational red shift by the interference of matter waves. Nature. 2010;463:926–9.
[4] Müller H, Stanwix P, Tobar M, Ivanov E, Herrmann S, Senger A, et al. Tests of relativity by complementary rotating Michelson-Morley experiments. Phys Rev Lett. 2007;99:050401.
[5] Luo J, Sheng L, Duan H, Gong Y, Hu S, Ji J, et al. TianQin: a space-borne gravitational wave detector. Class Quantum Gravity. 2016;33(3):035010.
[6] Chou CW, Hume DB, Rosenband T, Wineland DJ. Optical clocks and relativity. Science. 2010;329:1630–3.
[7] Millo J, Magalhaes DV, Mandache C, Coq YL, English EML, Westergaard PG, et al. Ultrastable lasers based on vibration insensitive cavities. Phys Rev A. 2009;79:053829.
[8] Chen L, Hall JL, Ye J, Yang T, Zang E, Li T. Vibration-induced elastic deformation of Fabry-Perot Cavities. Phys Rev A. 2006;74:053801.
[9] Nazarova T, Riehle F, Sterr U. Vibration-insensitive reference cavity for an ultra-narrow-linewidth laser. Appl Phys B. 2006;83:531–6.
[10] Webster SA, Oxborrow M, Gill P. Vibration insensitive optical cavity. Phys Rev A. 2007;75:011801.

[11] Argence B, Prevost E, Lévèque T, Le Goff R, Bize S, Lemonde P, et al. Prototype of an ultra-stable optical cavity for space applications. Opt Express. 2012;20:25409–20.
[12] Leibrandt D, Bergquist J, Rosenband T. Cavity-stabilized laser with acceleration sensitivity below 10^{-12} g^{-1}. Phys Rev A. 2013;87:023829.
[13] Leibrandt DR, Thorpe MJ, Notcutt M, Drullinger RE, Rosenband T, Bergquist JC. Spherical reference cavities for frequency stabilization of lasers in non-laboratory environments. Opt Express. 2011;19:3471–82.
[14] Häfner S, Herbers S, Vogt S, Lisdat C, Sterr U. Transportable interrogation laser system with an instability of mod $\sigma_y = 3 \times 10^{-16}$. Opt Express. 2020;28(11):16407–16.
[15] Chen Q, Nevsky A, Cardace M, Schiller S, Legero T, Häfner S, et al. A compact, robust, and transportable ultra-stable laser with a fractional frequency instability of 1×10^{-15}. Rev Sci Instrum. 2014;85:113107.
[16] Xu G, Jiao D, Chen L, Zhang L, Dong R, Liu T, et al. Analysis of vibration sensitivity induced by the elastic deformation of vertical optical reference cavities. IEEE Access. 2020;8:194466–76.
[17] Webster S, Gill. P. Force-insensitive optical cavity. Opt Lett. 2011;36(18):3572–4.
[18] Tao B, Chen Q. A vibration-sensitive-cavity design holds impact of higher than 100g. Appl Phys B. 2018;124:228.
[19] Chen X, Jiang Y, Li B, Yu H, Jiang H, Wang T, et al. Laser frequency instability of 6×10^{-16} using 10-cm-long cavities on a cubic spacer. Chin Opt Lett. 2020;18:030201.
[20] Cao J, Wang S, Yuan J, Liu D, Shu H, Huang X. Integrated multiple wavelength stabilization on a multi-channel cavity for a transportable optical clock. Opt Express. 2020;28(8):11852–60.
[21] Xu G, Jiao D, Chen L, Zhang L, Dong R, Liu T, et al. Vibration modes of a transportable optical cavity. Opt Express. 2021;29(15):24264–77.
[22] Herbers S, Häfner S, Dörscher S, Lücke T, Sterr U, Lisdat C. Transportable clock laser system with an instability of 1.6×10^{-16}. Opt Lett. 2022;47:5441–4.
[23] Xiao R, Xu Y, Wang Y, Sun H, Chen Q. Transportable 30 cm optical cavity based ultrastable lasers with beating instability of 2×10^{-16}. Appl Phys B. 2022;128:220.
[24] Jiao D, Deng X, Gao J, Zhang L, Xu G, Liu T, et al. Highly vibration-resistant sub-Hertz ultra-stable laser passing over 1700 km transport test. Infrared Phys Technol. 2023;130:104608.
[25] Häfner S, Falke S, Grebing C, Vogt S, Legero T, Merimaa M, et al. 8×10^{-17} fractional laser frequency instability with a long room-temperature cavity. Opt Lett. 2015;40:2112–5.
[26] Matei DG, Legero T, Häfner S, Grebing C, Weyrich R, Zhang W, et al. 1.5 μm Lasers with Sub-10 mHz Linewidth. Phys Rev Lett. 2017;118:263202.
[27] Cole GD, Zhang W, Martin MJ, Ye J, Aspelmeyer M. Tenfold reduction of Brownian noise in high-reflectivity optical coatings. Nat Photonics. 2013;67:46–650.
[28] Xu G, Zhang L, Liu J, Gao J, Chen L, Dong R, et al. Estimation of thermal noise for spindle optical reference cavities. Opt Commun. 2016;360:61–7.
[29] Robinson JM, Oelker E, Milner WR, Kedar D, Zhang W, Legero T, et al. Thermal noise and mechanical loss of SiO_2/Ta_2O_5 optical coatings at cryogenic temperatures. Opt Lett. 2021;46:592–5.
[30] Xu G, Jiao D, Chen L, Zhang L, Dong R, Liu T, et al. Thermal noise in cubic optical cavities. Photonics. 2021;8:261.
[31] Taguchi G. Introduction to Quality Engineering. Tokyo: Asian Productivity Organization; 1990.
[32] Hafiz MA, Ablewski P, Masoudi AA, Martínez HÁ, Balling P, Barwood G, et al. Guidelines for developing optical clocks with 10-18 fractional frequency uncertainty; 2019. https://arxiv.org/abs/1906.11495.
[33] Jiao D. Research on Key Technologies of Engineering Ultrastable Laser in Communication Band and its Application. China: University of Chinese Academy of Sciences; 2020.
[34] Newell DB, Richman SJ, Nelson PG, Stebbins RT, Bender PL, Faller JE, et al. An ultra-low-noise, low-frequency, six degrees of freedom active vibration isolator. Rev Sci Instrum. 1997;68:3211–9.
[35] Álvarez MD. Optical cavities for optical atomic clocks, atom interferometry and gravitational-wave detection. England: National Physical Laboratory and University of Birmingham; 2018.